Available online at www.sciencedirect.com

SciVerse ScienceDirect

Energy Procedia 00 (2013) 000–000

Energy Procedia

www.elsevier.com/locate/procedia

SolarPACES 2013

Uncertainty analysis of heliostat alignment at the Sandia solar field

Rachel Hogan[a], John Pye [a], Clifford Ho[b] and Edward Smith[b]

[a]*Australian National University, Canberra, Australia.*
[b]*Sandia National Laboratories, Albuquerque, USA.*

Abstract

Low-cost heliostats with open-loop tracking systems require careful calibration in order to track the sun accurately. This calibration can be done by mechanical adjustment, which increases the cost of both the components and commissioning, or it can be done automatically, using software, by 'learning' the various forms of misalignment present in a particular heliostat, and adjusting the pointing directions in order to cancel out the effect of those misalignments. A large set of training data will allow these corrections to be determined to quite high accuracy, and several of low-cost heliostat concepts have already been developed which make use of some form of this principle to reduce overall CSP system cost, though the methods used have not been thoroughly described in open literature.

The current study builds upon earlier work by Baheti and Scott (1980), Khalsa et al (2011) and Pye and Zhang (2012), to analyze the process of automated misalignment correction with the introduction of an uncertainty analysis applied to an experimental training data set. The accuracy of correction process from this experimental data is quantified, allowing a criterion to be applied to determine whether or not sufficient training has been completed for each heliostat to mean overall field accuracy requirements.

To investigate the potential improvements from extended training, a synthetic data set is generated, and used to investigate preferred times of year and times of data for training specific heliostats in the field. Summer data is shown to be best, but the additional of some winter data is helpful. Time-of-day is also important, especially for the sides of the heliostat field; middle-of-the-day training and spring or autumn training are seen to be less effective. A training programme for the entire heliostat field is presented and discussed: each heliostat is trained daily in summer for two minutes, and daily in winter for one minute in the morning and evening, resulting in 95% certainty that all heliostats will have their focal spot within 1.5 m of the target for the entire year, by an entirely automated process.

Selection and peer review by the scientific conference committee of SolarPACES 2013 under responsibility of PSE AG.

Keywords: solar thermal; heliostat, training data; numerical modelling; synthetic data

1. Introduction

Efficient operation of central tower solar concentrators depends on heliostats that can be accurately oriented to direct reflected light to the desired location on the receiver, thereby minimizing 'spillage' losses and ensuring optimal flux uniformity on the receiver. Baheti and Scott (1980) provided a method for automatic heliostat alignment based on a simple geometric model of a heliostat and its tracking mechanism. The geometric model had a number of misalignment parameters associated with angles and orientations of its components; by gathering experimental

Selection and peer review by the scientific conference committee of SolarPACES 2013 under responsibility of PSE AG.

'training' data on the location of a the heliostat focal spot on a target over a period of time, the misalignment parameters could be inferred through linear regression. The tracking algorithm can then be adjusted to correct for the effect of the misalignments. This method was recently improved and tested (Khalsa et al, 2011) and then implemented across the entire heliostat field at Sandia National Laboratories (Smith and Ho, 2013). Zhang and Pye (2012) made a simulation study of heliostat alignment including uncertainty analysis, but up to now this analysis has not be applied to an experimental data set. In this paper, we present the application of this uncertainty analysis to experimental data from Sandia. Given a training data set, we can estimate the misalignment parameters, together with a confidence interval on those values. We can propagate the analysis through a forecast annual simulation of the heliostat spot location and determine if, after correction, the heliostat spot can be guaranteed to remaining with a designed distance of the target. We can therefore decide, on a heliostat-by-heliostat basis, whether we have enough training data to achieve a specified solar field performance target. We can also use this information to schedule training at times when it will be of high value, such as at the ends of the day and at the solstices, when the heliostat angles are at the limits of their ranges.

2. Nomenclature

$\boldsymbol{\varepsilon}$	Vector of eight geometric misalignment parameters
θ	Azimuth angle
α	Elevation angle
Δ	Error in…
δ	Uncertainty in…
s^2	Variance of least squares fit
q_i	Azimuth and Elevation error matrix for measurement at time-step *i*
H_i	Geometric coefficient matrix for measurement at time-step *i*
C_{ij}	Covariance (see Section 4.1)

3. Sandia heliostat field

The heliostat field used for testing is the Sandia field in Albuquerque with supplied training data from Edward Smith. The heliostat field consists of 196 heliostats of the 'tee' type geometry, with a central support post, azimuth drive, and then a horizontal axis with elevation drive. The eight heliostats selected for detailed consideration in this study are indicated on Figure 1. These heliostats give a good indication of how the field performs as they are distributed throughout the field with comparison of east and west able to be monitored.

Figure 1: The heliostats circled in red show the location of analysed heliostats. BCS: Beam Characterisation System/target. (Smith and Ho, 2013)

3.1. Training data

The Baheti & Scott (1980) method for heliostat alignment requires gathering of a large set of data giving the location of the heliostat focal spot on the plane of a target, for a range of different dates and times. For this paper, data was gathered on the days: 2011: November (23rd) and 2012: April (21st, 30th), May (1st), August (9th, 21st, 27th), October (22nd, 25th, 29th). The information obtained for each sample point contained: date and time (by local clock), azimuth error, elevation error, intended mirror azimuth, and intended mirror elevation.

4. Analysis of experimental data

4.1. Calculation of misalignment parameters and uncertainties

According to the method described by Khalsa et al, 2011, the geometry of the misaligned heliostat is defined by eight misalignment parameters. When the geometry of the heliostat was analyzed with small angle approximations for all of these misalignments, the heliostat behavior can be reduced to a linear equation relating the errors in the azimuth and elevation directions ($\Delta\theta$ and $\Delta\alpha$) to each of the misalignment parameters, vector $\boldsymbol{\varepsilon}$. The linear coefficients are functions only of intended (or commanded) azimuth and elevation angles, θ and α. The value of the misalignment parameter vector $\boldsymbol{\varepsilon}$ is determined by linear regression using both the azimuth error and elevation error data simultaneously. As discussed by Zhang and Pye (2012) and earlier by Khalsa et al (2012), the linear regression is solved; variance and covariance matrix are then calculated, leading to uncertainty values $\delta\varepsilon_i$ for each misalignment parameter ε_i, defined as two standard deviations in size. The calculations implemented for the rest of this paper are as a script in the Python language, using NumPy routines for matrix algebra.

4.2. Spot location offset from target and uncertainty

Results from the calculation of values in the section 4.1 allow calculation of heliostat azimuth and elevation errors arising from the misalignment parameters. To translate these angular errors into errors in spot location on the target plane, vector geometry is used. Essentially, the offset (misaligned) heliostat pointing direction is calculated by adding the azimuth and elevation errors to the 'command' angles θ and α and converted to a directional unit vector; that offset heliostat angle is then used to calculate a deflected beam direction, and the intersection of the deflected beam with the target plane can then be readily calculated. The uncertainties in the heliostat azimuth and elevation angles $\delta\theta$ and $\delta\alpha$ can also be calculated, by substituting the uncertainties $\delta\boldsymbol{\varepsilon}$ in place of $\boldsymbol{\varepsilon}$. These two uncertainties were translated, individually, into offsets on the target plane using the same ray/plane intersection method as above. The maximum offset of the two focal spots (i.e. with either the azimuth uncertainty added or the elevation uncertainty added) was used to define an uncertainty radius around the spot location, which represents a 95% certainty that the spot will fall within that radius.

4.3. Heliostat Accuracy as figure of merit

A figure of merit of heliostat training accuracy is determined by calculating the maximum displacement from the target of the spot locations with the added value of the uncertainty radius around that point (outlined in section 4.2). This value represents the maximum possible offset distance from the target, with 95% certainty, for any spot aimed at the target from that heliostat in future. Values shown in Table 1 show the number of training spots, the uncertainty of the spot location, and the overall heliostat accuracy. Examples of the field extremes and their spot locations are shown in Figure 2.

One specific heliostat, 12E13, was deliberately misaligned by insertion of shims. The effect of serious misalignment will be most evident for that heliostat, as will be the effect of alignment correction. The results shown for 12E13 in clearly show the need for alignment correction due to the large distance of the uncorrected spots from the target, a distance of 2 m or more. The other heliostats near the outer edge of the field (including 05E09 and 05W09) also show spot locations up to one meter off target; these heliostats would also benefit from alignment correction. The uncertainty radius for 12E13 is the lowest due to the larger number of training data spots for analysis. While 10E01 does not have the smaller number of data points, in the data it was found to have an outlier. The outlier is removed during further modeling.

The training data set analyzed here can therefore be seen to provide a radius of uncertainty of at least two meters, a distance which it would be desirable to be able to reduce. The only way to reduce the uncertainty arising from this training data is to gather more training data, possibly being strategic about the times when the training data is collected.

Table 1: Experimental results of eight selected heliostats showing number of training spots, uncertainty radius, and heliostat accuracy.

	Training spots	Uncertainty radius	Heliostat Accuracy		Training spots	Uncertainty radius	Heliostat Accuracy
05E01	135	5.88 m	6.12 m	05W01	122	3.05 m	3.14 m
05E09	136	5.35 m	6.27 m	05W09	134	3.75 m	4.32 m
10E01	578	7.95 m	8.19 m	10W01	187	6.05 m	7.12 m
12E13	1178	2.93 m	6.18 m	12W13	178	4.78 m	5.18 m

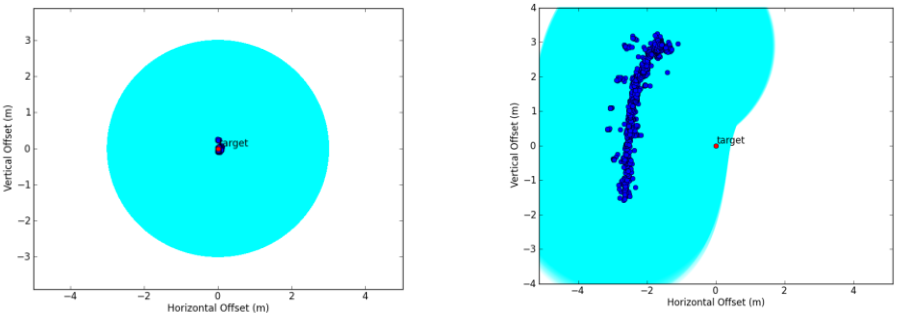

(a) 05W01 (b) 12E13

Figure 2: Spot locations of training data (dark blue spot) for heliostat (a) 05W01 and (b) 12E13 with certainty of 95% of spots falling within the uncertainty radius (light blue) surrounding each plotted spot.

4.4. Forecasting and correcting heliostat location using misalignment parameters

It is possible to calculate the effect of heliostat misalignment on the focal spot location on the target for arbitrary future dates and times using the misalignment parameters calculated above. This least squares fit will not take into account the spread of the data from effects such as wind, with the result that they are far more regular in their arrangement that the training data. The fit for heliostat 12E13 (chosen to show calibration as it had a deliberate misalignment introduced by mechanical insertion of shims in the support frame) can be seen in Figure 4 (a).

4.4.1. Including effects of wind scatter

As it is this wind scatter that leads to the genuine uncertainty in forecast spot location, any attempt to simulate the effect of gathering longer-duration training-data sets must also add a synthesized form of wind scatter. A normal distribution is assumed, with mean and standard deviation equal to that found for the training data set. The residual values for the linear regression fit were collated and the mean and standard deviation for both the azimuth and the elevation were found. For 12E13, these values are: azimuth mean (0.0000), azimuth standard deviation (0.0005), elevation mean (0.0000), and elevation standard deviation (0.0004). The histogram of residuals for the azimuth and elevation is shown in Figure 3 and demonstrates a near normal distribution centered around 0.

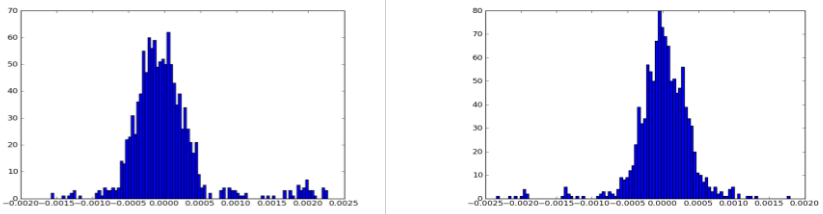

(a) (b)

Figure 3: Histograms of (a) Azimuth and (b) elevation residuals spread in radians from the training data compared to the least squares fit

The original least squares fit parameters as well as the included effects of wind scatter are shown in Figure 4. The forecast spot locations are for one-minute time steps between 9 am and 5 pm on the 21st day of each month in the

year. The individual mean and standard deviation values are tailored to each heliostat and are affected by the distance between the heliostat and target. However, they do not take into account the difference between morning/evening and seasonal winds. Further climate research is required to predict the spread with a higher accuracy.

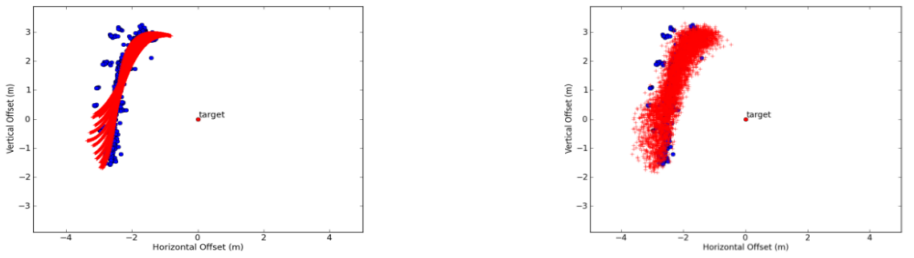

(a) (b)

Figure 4: Heliostat 12E13 with the target location, training data spot locations (blue dot), and synthetic data used from fitted parameters with (a) least squares fit parameters and (b) random wind error included for one day each month over a year at each minute between 9am-5pm (red cross).

4.5. Applying the corrections

These deflected spot locations with spread can now be corrected by applying a numerical solution method, a two-variable Newton's method was used to solve f_1 and f_2 for zero. Thus, given a desired azimuth and elevation angle (θ and α, respectively), we can solve for the "compensated" angles (θ' and α') that you must command the system to, to get the beam where you want. Iteration by this method is required as the errors are not linearly correlated.

$$f_1 = -\varepsilon_1 \sin\theta' \tan\alpha' - \varepsilon_2 \cos\theta' \tan\alpha' - \varepsilon_3 - \varepsilon_5\theta' - \varepsilon_7 \tan\alpha' - \frac{\varepsilon_8}{\cos\alpha'} - \theta' + \theta \quad (1)$$

$$f_2 = -\varepsilon_6\,\alpha' - \varepsilon_1 \cos\theta' + \varepsilon_2 \sin\theta' + \alpha - \alpha' - \varepsilon_4 \quad (2)$$

5. Analysis of synthetic training data

To determine how much training data is appropriate, a set of synthetic data was generated for times throughout the year based on the values of the epsilon matrix as generated by the training data as well as the spread calculated for the azimuth and elevation for each individual heliostat.

5.1. Correction of synthetic data

Correction of the synthetic data as outlined in section 4.5, requires wind/random error to be applied to the uncorrected synthetic data as well as the corrected synthetic data. The synthetic data shown in this section is for the hours of 9am-5pm (time step each minute) for the 21st of each month throughout 2012. Table 2 shows the results for the eight selected heliostats with corrections. For comparison of the experimental data, the plots of 05W01 and 12E13 are shown in Figure 5.

Table 2: Synthetic results for the 21st of each month in the year between hours 9am-5pm with one time step each minute for eight selected heliostats showing number of training spots, uncertainty radius, and heliostat accuracy after corrections applied.

	Uncertainty radius		Uncertainty radius
05E01	0.34 m	05W01	0.17 m
05E09	0.33 m	05W09	0.19 m
10E01	0.27 m	10W01	0.34 m
12E13	0.77	12W13	0.51

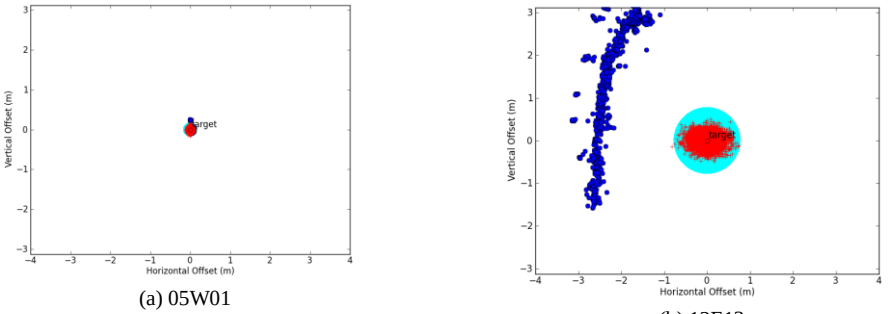

(a) 05W01 (b) 12E13

Figure 5: Spot locations of training data (dark blue spot) compared to synthetic corrected data (red cross) for heliostat (a) 05W01 and (b) 12E13 with a certainty of 95% of spots falling within the uncertainty radius (light blue) surrounding each plotted cross.

The results show corrections with an overall uncertainty radius of less than one meter and heliostat accuracy less than 1.5 meters. Therefore, testing for one day each month shows a large improvement over the current training data obtained from the Sandia Laboratories.

The best time of year, day and period was determined to obtain a field of satisfactory training data for the performance of the field. Due to the large uncertainty associated with 12E/W13, they were used to determine how to minimize the uncertainty. A heliostat was selected on each side to determine whether morning/evening effects affected the data.

5.1.1. Time of year

Three consecutive days around the solstices and equinoxes were selected for analysis of time of year training. The time of day selected is 9am-5pm so the winter data does not have significantly less data points.

Table 3: Seasonal training: Dark Blue spot = training data, Red cross = corrected synthetic data with wind error and seasonal variation, 95% certainty of spots falling within the uncertainty radius (light blue) over the time period 9am-5pm.

		Spring March 21st-23rd 2012	Summer June 21st-23rd 2012	Autumn September 21st-23rd 2012	Winter December 21st-23rd 2012
Uncertainty Radius	12E13	11.32 m	9.12 m	11.61 m	17.70 m
	12W13	6.95 m	5.25 m	7.12 m	9.54 m

The results show that training for the same number of days in summer has only about half of the uncertainty of that period in winter. These results also take into account the same number of training spots. Therefore, if training can only be carried out during one time of the year, the summer period will give more significant results for the same number of time steps. The heliostat 12E13 also shows higher levels of uncertainty due to the increased spread from the shims inserted to obtain the training data.

5.1.2. Combining time periods

A combination of summer and winter data was also used to show what effect taking sample points from various times of the year had on the overall result. These results also show the how increasing the sample points by a couple of days reduces the uncertainty for 12E13 (heliostat accuracy: three summer days = 9.35m, five summer days = 7.53m). The time periods selected were from 9am-5pm. The results show that the best results are obtained with majority summer data and at least some winter data points included. There is also the conclusion that if majority of training is carried out in the winter period with only a bit of summer data, it will still have more accuracy than only using one season to gather data.

Table 4: Combination of summer and winter data for hours 9am-5pm on days nominated

Summer Days (June)	Winter Days (December)	Uncertainty Radius (m)
20th-24th	N/A	6.98
20th-23rd	22nd	1.06
21st-23rd	22nd-23rd	1.07
21th-22nd	21st-23rd	1.15
22nd	21st-24th	1.37
N/A	20th-24th	13.71

5.1.3. Time of day

Various blocks of hours were selected in Table 5 and show when training should be carried out for the most efficient data collection. To compare the field, the summer data was also found for 05E/W01. The results show that the optimum timing occurs at the same time for two extremes within the heliostat field, which occur around sunrise and sunset for all heliostats and training hours are the same for heliostats at the inner center of the field as well as the outer edge heliostats. During summer, training should be carried out between the hours of 6-9am for the heliostats on the East side of the tower. The Western heliostats in summer should be trained in the evenings between 5-8pm. The heliostats close to the center line of the field can potentially be trained in the mornings or evenings as they are less sensitive to the sun location. During winter, the training should also be carried out around sunrise and sunset. Data obtained during the middle of the day in winter will not provide much significance to the uncertainty and should not be carried out to avoid unnecessarily using resources. The method used to calculate Table 5 is based on simplistic assumptions about wind and will tend to be overly conservative. Further work is intended to include correlation of some wind effects and should result in further tightening of the forecast heliostat accuracy for these cases.

Table 5: Uncertainty radius based on different training times throughout the day in summer and winter for 12E/W13. Red X: Should not train. Green **: Optimum training time. Yellow *: Reasonable training time

	Heliostat Accuracy (m)					
	Summer (June)				Winter (December)	
Time of day (each day during month)	12E13	12W13	05E01	05W01	12E13	12W13
5-8	9.10*	16.27	6.36*	3.61	87.60 X	235.27
6-9	8.29**	13.01	5.55**	2.99*	30.03	29.62
7-10	11.26*	13.19	6.55*	3.26	18.46**	16.29*
8-11	19.89	13.40	7.66	3.61	23.51	17.91*
9-12	57.39 X	13.07	10.29 X	4.25	45.94	23.75
10-13	50.54 X	12.90	16.75 X	5.67 X	143.87 X	41.43 X
11-14	26.92 X	14.08	72.04 X	10.59 X	54.23 X	202.17 X
12-15	21.51	17.05	25.70 X	34.18 X	32.92	53.37 X
13-16	19.70	29.83 X	12.93 X	8.99 X	25.27	21.87
14-17	19.01	83.12 X	9.61	5.41 X	22.44*	15.69**
15-18	18.47	20.04	8.04	4.16	38.72	29.08
16-19	16.87	9.69*	7.16*	3.40	135.94 X	152.68 X
17-20	14.88	5.65**	6.15*	2.98**	N/A	N/A
18-21	21.12	8.65*	8.59	4.08	N/A	N/A

6. Suggested training schedule

The maximum heliostat accuracy that was deemed acceptable was 1.5 meters; selected arbitrarily and further investigation for cost optimization should be carried out to confirm. For the 196 heliostats, the majority of training should occur in the summer. During the three summer months (June, July, August) the eastern half should be trained in the mornings and the western half should be trained in the evenings. Over the three hour optimum period (detailed in section 5.1.3), this allows for ~2 minutes per heliostat. All previous information presented has been based on the principle of one time calculation per minute. Based on the training data from Sandia, it is feasible to take up to eight measurements per minute. Measurements should be taken during winter as well, with morning and evening data.

Using only one minute in the morning and one in the evening allows for the opposite side of the field to get morning/evening data within optimum time. All training data has 2744 data samples with training on the eastern side: June to August (9:00-9:02am), December to February (7:15-7:16am and 4:45-4:46pm) and the western side: June to August (5:00-5:02pm), December to February (7:15-7:16am and 4:45-4:46pm).

Table 6: Results of suggested training schedule for eight selected heliostats

	Uncertainty radius	Heliostat accuracy	Uncertainty ratio		Uncertainty radius	Heliostat accuracy	Uncertainty ratio
05E01	0.92 m	1.00 m	0.0109 m/m	05W01	0.39 m	0.45 m	0.0088 m/m
05E09	0.33 m	0.51 m	0.0026 m/m	05W09	0.28 m	0.33 m	0.0058 m/m
10E01	0.78 m	0.94 m	0.0060 m/m	10W01	0.86 m	0.92 m	0.0072 m/m
12E13	0.90	1.18	0.0040 m/m	12W13	0.67	0.82	0.0043 m/m

In general, the heliostat accuracy is larger for heliostats along the center of the field than the heliostats on the outer edges. This can be seen by the smaller heliostat accuracy for 05E09 (0.51m) compared to the radius for 05E01 (1.00). When the uncertainty radius is divided by the distance between the heliostat and the target (Uncertainty ratio), it shows there is little difference between the rows with heliostats in the same column. However, there is a significant increase in the error ratio in any row when the heliostat is close to the center (aka xxE/W01). The suspected reason for this is the smaller changes in angle throughout the day for the same amount of noise/generated error. Therefore training is most effective for heliostats on the edge of the field, yet the spot locations of the heliostats along the center are less effected by error due to the smaller distance between the tower and the heliostat. The change in angle: noise ratio is also the reason training is most effective around sunrise and sunset; there is a greater change in sun location for each time step compared to the change in noise/error.

7. Conclusions

The model was able to successfully predict the uncertainty radius and predicted offset from target (addition of values equaling the heliostat accuracy) for eight representative heliostats in the Sandia field with values of less than 1.5m within a training time period for the whole field restricted to mornings and evenings in summer and winter only. The correction model created is able to use real training data supplied by Sandia National Laboratories to create a set of error epsilon values based on an equation provided by Khalsa et al [1]. This set of epsilon values can be used with time intervals throughout the year with corresponding sun angles and the required heliostat orientations to create a set of synthetic data. The synthetic data has random error applied to it to account for wind and other random errors. For the 196 heliostats, a minute of training for each will take just over three hours; if the field is separated into east and west training times, two minutes of training can be conducted per heliostat. After analysis of time/seasonal training periods, the results show that the best training occurs in summer, where the Eastern half of the field should occur in the mornings between 6-9am and the Western half of the field should have training in the evenings between 5-8pm. Two minutes per heliostat, with eight readings per minute, on each day during June-August should be sufficient summer data. Both sides of the field should obtain winter data to reduce the uncertainty. One minute of data in the morning and evening, with eight measurements per minute, during December-February for each heliostat should be sufficient training when combined with the summer data. Training is most effective for the heliostats on the edge of the field due to the greater change in angle for each time step compared to the noise created by wind and other random errors.

References

[1] S S Khalsa, C K Ho and C E Andraka, 2011, An Automated Method to Correct Heliostat Tracking Errors. Proceedings of SolarPACES, Granada, Spain, Sept 20-23.

[2] Baheti, R.S. and P.F. Scott, 1980, “Design of Self-Calibrating Controllers for Heliostats in a Solar Power Plant,” IEEE Trans. Autom. Control, Vol. AC-25, No. 6, pp. 1091-1097.

[3] Zhang, J, Pye, J.D. and Ho, C.K., 2012, Estimation of Uncertainty in Automated Heliostat Alignment. Proceedings of the 50th annual Australian Solar Energy Society conference, ‘Solar 2012’, Melbourne, December.

[4] Smith, E. Ho, C. 2013. Field Demonstration of an Automated Heliostat Tracking Correction Method.